



HAL
open science

Non-intrusive Diagnosis of a PEMFC

Melika Hinaje, Olivier Béthoux, Guillaume Krebs, Bernard Davat

► **To cite this version:**

Melika Hinaje, Olivier Béthoux, Guillaume Krebs, Bernard Davat. Non-intrusive Diagnosis of a PEMFC. IEEE Transactions on Magnetics, 2015, 51 (3), <https://ieeexplore-ieee-org.bibliopam.supelec.fr/stamp/stamp.jsp?tp=&arnumber=7093443>. 10.1109/TMAG.2014.2355497 . hal-01238492

HAL Id: hal-01238492

<https://hal.science/hal-01238492>

Submitted on 5 Dec 2015

HAL is a multi-disciplinary open access archive for the deposit and dissemination of scientific research documents, whether they are published or not. The documents may come from teaching and research institutions in France or abroad, or from public or private research centers.

L'archive ouverte pluridisciplinaire **HAL**, est destinée au dépôt et à la diffusion de documents scientifiques de niveau recherche, publiés ou non, émanant des établissements d'enseignement et de recherche français ou étrangers, des laboratoires publics ou privés.

Non-intrusive Diagnosis of a PEMFC

Melika Hinaje¹, Olivier Bethoux², Guillaume Krebs², Bernard Davat¹

¹Université de Lorraine – GREEN, F-54518 Vandoeuvre Cedex, France

²LGEP (CNRS UMR 8507), F-91192 Gif sur Yvette, France

melika.hinaje@univ-lorraine.fr

Abstract— Many reasons may cause malfunction of a proton exchange membrane fuel cell stack. Moreover, a single defect cell can affect the whole stack functioning, therefore the localization of this cell is crucial as well as identifying the root causes for such malfunctioning. The diagnosis tool has to be non intrusive and to be easy to replicate to a new fuel cell system. This paper explores paths to achieve such monitoring based on the use of the magnetic field induced by the fuel cell stack internal currents. Designing and using a three-dimensional simulation tool allows to establish a cause and effect relationship between fuel cell defects and specific magnetic signatures. This preliminary work enables to determine the required magnetic sensor accuracy, the sensor orientation and location as well as the experimental precautions for relevant measurements.

Index Terms— Proton exchange membrane fuel cell; Maxwell-Stefan diffusion; magnetic field; 3D PDE modeling, diagnosis.

I. AIM

Using polymer electrolyte membrane (PEM) fuel cells (FCs) is an attractive way to produce energy without greenhouse gas. A defect in the FC stack, such as drying, flooding, starvation, active layer deterioration, induces major negative effect on the operation of the overall energy conversion system (FC and its auxiliaries): performance decreases and may cause the FC system to shut down, with possible damages to the PEMFC or to one of the auxiliaries. Identification of the defect and understanding the physical processes involved are essential to diagnose accurately the reduced performance causes. The aim of this work is to compute the magnetic field created by a PEMFC in order to identify a specific signature in case of malfunctioning cell.

II. PEMFC MODELING

To predict the FC performance, the unknowns, w_{H_2} , $w_{H_2O,a}$, $w_{H_2O,c}$, w_{O_2} , w_{N_2} , p_a , p_c , ϕ_m , ϕ , and \mathbf{v} have to be computed by solving the equations of mathematical physics that describe the overall cell; computational domain is given in Fig. 1.

It is assumed that:

- Three species oxygen, nitrogen and water are present on the cathode side, while hydrogen and water are considered in the anode side.
- The PEMFC is operating in steady state.
- Flow is considered laminar.
- There is no condensation in the cell. The single phase model described here is sufficient for modelling the mass transport in the porous anode and cathode up to moderately high current densities [1] [2].
- The FC temperature remains constant and homogeneous all over the cell.
- The membrane is gas-tight.
- The channels are approximated by straight channels.

TABLE I NOMENCLATURE

| Symbol | Quantity |
|----------------|---|
| A | Magnetic vector potential [Wb. m ⁻¹] |
| B | Magnetic flux density [T] |
| C _i | Concentration of species i [mol.m ⁻³] |
| D_{ij}^{eff} | Diffusion coeff. of species i in the species j [m ² .s ⁻¹] |
| $D_{H_2O}^m$ | Diffusion coefficient of water [m ² .s ⁻¹] |
| EW | Equivalent weight of membrane [g.mol ⁻¹] |
| F | Faraday constant, 96485 [C.mol ⁻¹] |
| H | Magnetic field [A.m ⁻¹] |
| I | Current [A] |
| J_{cell} | Current density [A.m ⁻²] |
| L_d | GDLs thickness [m] |
| L_m | Membrane thickness [m] |
| M_i | Molar mass of the species i [kg.mol ⁻¹] |
| P_i | Partial pressure of species i [Pa] |
| P_{sat} | Saturated pressure [Pa] |
| P_T | Total pressure ($P = \sum P_i$) [Pa] |
| $P_{a,c}$ | Pressure of the gas mixture at anode or cathode side |
| R | Universal gas constant, 8,314 [J. mol ⁻¹ .K ⁻¹] |
| RH | Relative humidity |
| T_{pile} | Temperature of the fuel cell [K] |
| x_i | Molar fraction of species i |
| \mathbf{v} | Velocity [m.s ⁻¹] |
| w_i | Mass fraction of species i |
| z | Length [m] |
| Greek symbols | |
| α | Transfer coefficient |
| ε | porosity |
| ϕ | Potential [V] |
| $\mu_{a,c}$ | Coefficient of viscosity of the gas mixture [Pa.s] |
| μ | Permeability magnetic [H. m ⁻¹] |
| λ | Water content in the membrane |
| ρ_{dry} | Dry density of membrane [g.m ⁻¹] |
| $\rho_{a,c}$ | Density of the mixture [kg.m ⁻³] |
| σ_{H^+} | Electric conductivity of the membrane [S.m ⁻¹] |
| Subscript | |
| a | anode |
| act | activation |
| c | cathode |
| CL | Catalyst layer |
| e | Electrode |
| GDL | Gas diffusion layer |
| i | Species (H ₂ , H ₂ O, O ₂ , N ₂) |
| in | Inlet |
| OCV | Open circuit voltage |
| out | Outlet |
| Superscript | |
| eff | Effective |
| 0 | Standard conditions |

A. Mass and Momentum balances (coupled)

In anode and cathode sides, the transport phenomena are similar, only the species differ. In channels, the velocity \mathbf{v} and the pressure of the gas mixtures are described by Navier-Stokes equations, i.e. the conservation of momentum (1) and the conservation of mass known as mass continuity

equation (2). As GDL and CL are porous media, the Navier-Stokes equations have to be modified that leads to the so-called Brinkman equations [3] (3).

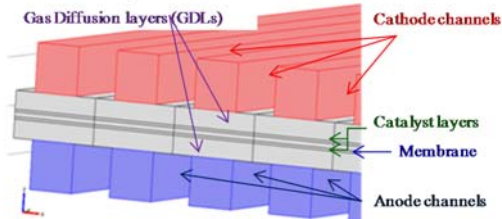


Fig. 1. Cell detail: zoom on the GDLs and the MEA.

In the channel, the following system has to be solved

$$\begin{cases} \nabla \cdot (\rho_{a,c} \mathbf{v}_{a,c} \otimes \mathbf{v}_{a,c} - \mu_{a,c} \nabla \mathbf{v}_{a,c}) = \nabla \cdot [\mu_{a,c} (\nabla \mathbf{v}_{a,c})^T] \\ \quad - \nabla \cdot \left(p_{a,c} + \frac{2}{3} \mu_{a,c} \nabla \cdot \mathbf{v}_{a,c} \right) = 0 & (1) \\ \nabla \cdot (\rho_{a,c} \mathbf{v}_{a,c}) = 0 & (2) \end{cases}$$

while in the GDLs and in the CLs the below-stated system of equations needs to be solved:

$$\begin{cases} \nabla \cdot \left(\frac{\rho_{a,c}}{\varepsilon_{GDL,CL}} \mathbf{v}_{a,c} \otimes \mathbf{v}_{a,c} - \frac{\mu_{a,c}}{\varepsilon_{GDL,CL}} \nabla \mathbf{v}_{a,c} \right) = \\ \nabla \cdot \left[\frac{\mu_{a,c}}{\varepsilon_{GDL,CL}} (\nabla \mathbf{v}_{a,c})^T \right] - \nabla \cdot \left(p_{a,c} + \frac{2}{3} \frac{\mu_{a,c}}{\varepsilon_{GDL,CL}} \nabla \cdot \mathbf{v}_{a,c} \right) - \frac{\mu_{a,c}}{\kappa_{GDL,CL}} = 0 & (3) \\ \nabla \cdot (\rho_{a,c} \mathbf{v}_{a,c}) = 0 & (4) \end{cases}$$

B. Mass and species balance

The mass and molar fractions obey the Maxwell-Stefan equations which describe the multi-species diffusion and convection in channels (5-6) and electrodes. Pair of species (i,j) interactions are characterized by the binary diffusion coefficient D_{ij} [4]: to account for the electrodes' porosity, the effective diffusion coefficient D_{ij}^{eff} (9) substitute the D_{ij} coefficient in relation (8).

$$\begin{aligned} \nabla \cdot \left[-\rho \cdot w_i \sum_{j=1}^e D_{ij} \left(\nabla x_j + (x_j - w_j) \frac{\nabla p_{a,c}}{p_{a,c}} \right) + w_i \rho \mathbf{v}_{a,c} \right] &= R_i \\ (5) \\ \mathbf{N}_i &= \left[-\rho \cdot w_i \sum_{j=1}^e D_{ij} \left(\nabla x_j + (x_j - w_j) \frac{\nabla p_{a,c}}{p_{a,c}} \right) + \rho \mathbf{v}_{a,c} w_i \right] & (6) \end{aligned}$$

Where ρ is the mixture density and D_{ij} is defined by:

$$\rho = \left(\sum_{i=1}^e x_i M_i \right) \frac{p_{a,c}}{RT} \quad (7)$$

$$D_{ij} = D_{ij}^0(p^0, T^0) \frac{p^0}{T^0} \left(\frac{T}{T^0} \right)^2 \quad (8)$$

In the GDLs and CLs into account, the effective diffusion coefficients are computed by the Bruggeman relation:

$$D_{ij}^{eff} = D_{ij} \varepsilon_{GDL,CL}^{3/2} \quad (9)$$

Using the Onsager reciprocal relation [5], [6] also leads to the following relation:

$$D_{ij}^{eff} = D_{ji}^{eff} \quad (10)$$

In the continuity equation (5), species production and consumption are represented by a source term (water production) and a sink term (reactant consumption) respectively. The corresponding R_i terms is expressed in $\text{kg}/(\text{m}^3 \cdot \text{s})$. Obviously $R_i=0$ in flow channels.

$$R_{O_2} = \frac{j_c}{4F} M_{O_2} \quad (11)$$

$$R_{H_2} = -\frac{j_a}{2F} M_{H_2} \quad (12)$$

$$R_{H_2O} = -\frac{j_c}{2F} M_{H_2O} \quad (13)$$

Where j_a and j_c are the transfer current densities at CLs.

TABLE II GEOMETRY PARAMETERS
(2)

| Parameters | Value |
|----------------------------------|-------------------|
| Active area | 100 cm^2 |
| Anode GDL thickness | 380 μm |
| Cathode GDL thickness | 380 μm |
| Membrane thickness | 100 μm |
| Anode catalyst layer thickness | 50 μm |
| Cathode catalyst layer thickness | 50 μm |
| GDL porosity | 0.4 |
| Catalyst layer porosity | 0.3 |
| Anode and cathode channel width | 1 mm |
| Anode and cathode channel depth | 1 mm |
| Cog height of bipolar plates | 0.9 mm |
| GDL conductivity | 220 S/m |
| Membrane conductivity | 10 S/m |

C. Redox reaction and produced current

Indeed, hydrogen oxidation leads to charges' displacements: a proton one occurs through the membrane inducing a ionic current j_{H^+} while electrons travel are conducted by the electrodes resulting in an electronic current, j_e . Current conservation is expressed as follows:

$$\nabla \cdot j_{\text{cell}} = \nabla \cdot j_e + \nabla \cdot j_{H^+} = 0 \quad (14)$$

Ohm's law links current j_i densities to potentials ϕ_i :

$$\nabla \cdot (-\sigma_e^{eff} \nabla \phi_e) = -j_{a,c} \quad (15)$$

$$\nabla \cdot (-\sigma_{H^+}^{eff} \nabla \phi_{H^+}) = j_{a,c} \quad (16)$$

In (15) and (16), the source terms j_i derive from the electrochemical reactions described by Butler-Volmer equation.

$$j_a = a_v j_o^{ref} \left(\frac{C_{H_2}}{C_{H_2}^{ref}} \right)^{1/2} \left[\exp\left(\frac{\alpha_a F}{RT}\right) \eta_{act} - \exp\left(-\frac{\alpha_c F}{RT}\right) \eta_{act} \right] \quad (17)$$

$$j_c = a_v j_o^{ref} \left(\frac{C_{O_2}}{C_{O_2}^{ref}} \right) \left[\exp\left(\frac{\alpha_a F}{RT}\right) \eta_{act} - \exp\left(-\frac{\alpha_c F}{RT}\right) \eta_{act} \right] \quad (18)$$

The reference exchange current j_o^{ref} depends on several parameters such as operating temperature and requires a large number of experiments [7-8] to be properly identified. η_{act} is the voltage drop between electrodes and electrolyte:

$$\text{At the anode side } \eta_{act} = \varphi_e - \varphi_{H^+} \quad (19)$$

$$\text{At the cathode side } \eta_{act} = \varphi_e - \varphi_{H^+} - V_{oc} \quad (20)$$

D. Boundary conditions

The boundary conditions have to be specified for all variables in each domain. In anode and cathode channels, inflows are given by their velocity and their inlet mixtures:

$$v_{a,c} = v_{a,c,in} \quad (21)$$

$$w_a = w_{H_2,in} \quad (22)$$

$$w_c = \begin{cases} w_{O_2,in} \\ w_{H_2O,in} \end{cases} \quad (23)$$

The outlet boundaries are given by:

$$p_{a,c} = p_{out} \quad (24)$$

and

$$-\mathbf{n} \cdot \left[\rho \cdot w_i \sum_{j=1}^e D_{ij} \left(\nabla x_j + (x_j - w_j) \frac{\nabla p_{a,c}}{p_{a,c}} \right) \right] = 0 \quad (25)$$

Elsewhere no slip conditions apply and no flux go out. Thus:

$$-\mathbf{n} \cdot \mathbf{N}_i = 0 \quad (26)$$

The potential is fixed at gas channel-gas diffusion layer interfaces:

$$\text{At the cathode side: } \varphi_e = V_{cell} \quad (27)$$

$$\text{At the anode side: } \varphi_e = 0 \quad (28)$$

$$\text{At the membrane: } \varphi_{H^+} = 0 \quad (29)$$

At the top and at the bottom and on the back and on the front of the FC unique cell, no current goes out. Hence:

$$-\mathbf{n} \cdot \mathbf{j}_e = 0 \quad (30)$$

$$-\mathbf{n} \cdot \mathbf{j}_{H^+} = 0 \quad (31)$$

E. Magnetic formulation

As discussed earlier, the main aim of this study is to propose a set of guiding principles that will support the implementation of non intrusive fuel cell malfunctioning detection. A defect in the heart of the fuel cell might modify the current density repartition and consequently the resulting magnetic field. After computing the fuel cell electrical operating point, the magnetic field is calculated by means of the magnetic vector potential (32).

In this part, the studied domain is the single fuel cell Ω_{FC} and the air around it Ω_a . The air domain dimensions are chosen much larger than the cell ones.

$$\Delta \mathbf{A} - \mu \mathbf{j} = \mathbf{0} \quad \text{in } \Omega_a \cup \Omega_{FC} \quad (32)$$

To ensure the uniqueness of the solution, a Coulomb gauge (33) has to be coupled to Poisson equation (32).

$$\nabla \cdot \mathbf{A} = 0 \quad (33)$$

F. Boundary conditions

The boundary surface is denoted by Γ_{air} . Zero Dirichlet boundary conditions can be applied.

$$\mathbf{A} = \mathbf{0} \quad \text{on } \Gamma_{air} \quad (34)$$

To obtain the PEMFC operating point (V, I), 3D coupling PDE, describing the mixture gas diffusion and the redox reactions, have to be solved under a given operating conditions. Subsequently, the resulting magnetic field is computed by means of MVP. All the equations have been implemented in FEM software.

III. SOME RESULTS

A. Defect cathode channel

The considered fuel cell features a 100 cm² active area. As one of its cathode channels is blocked, O₂ does no more diffuse correctly (Fig. 2) and consequently the electrochemical reaction as well as the current distribution are locally disturbed; finally the resulting magnetic field is modified (Fig. 3 and 4).

B. Defect anode channel

The same default is simulated at the anode side; a stopper at anode channel is located at the top or the middle of the single fuel cell as shown in Fig 5.

Indeed, due to the stopper, hydrogen diffuses hardly in the default channel. However for a specified current of 27A, as shown in Fig. 5, the same default at anode side does not alter significantly the magnetic field distribution compared to cathode side.

TABLE III OPERATING CONDITIONS

| Parameters | Value |
|---|--|
| Fuel cell temperature | 60 °C |
| Hydrogen flow rate | 624 mL/min |
| Air flow rate | 1.56 L/min |
| Inlet H ₂ mass fraction (anode) | 0.743 |
| Inlet O ₂ mass fraction (cathode) | 0.228 |
| Inlet H ₂ O mass fraction (cathode) | 0.023 |
| Anode inlet flow velocity | 0.2 m/s |
| Cathode inlet flow velocity | 0.5 m/s |
| Anode viscosity | 1.19 10 ⁻⁵ Pa/s |
| Cathode viscosity | 2.46 10 ⁻⁵ Pa/s |
| Porous electrode permeability | 1.18 10 ⁻¹¹ m ² |
| GDL permeability | 2.36 10 ⁻¹² m ² |
| H ₂ -H ₂ O binary D _{ij} | 1.055 10 ⁻⁴ m ² /s |
| O ₂ -N ₂ binary D _{ij} | 2.751 10 ⁻⁵ m ² /s |
| N ₂ -H ₂ O Binary D _{ij} | 2.951 10 ⁻⁵ m ² /s |
| O ₂ -H ₂ O binary D _{ij} | 3.233 10 ⁻⁵ m ² /s |
| Fuel cell voltage | From 0.9 V to 0.6 V |

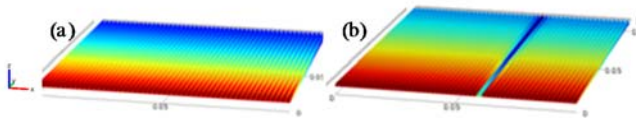
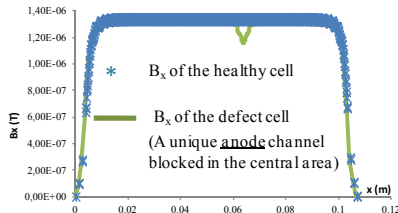
Fig. 2. O₂ diffusion: (a) healthy cell and (b) defective cathode channelFig. 3. Magnetic induction tangential component B_x at 0.6 V-31A.: xz view of (a) a healthy cell and (b) a defective cathode channel cell

Fig. 4. Comparison between the tangential component of the magnetic induction for a healthy and defective cathode channel

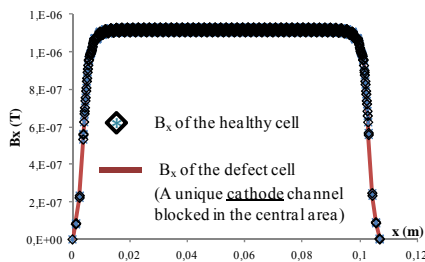


Fig. 5. Comparison between the tangential component of the magnetic induction for a healthy and defective anode channel

IV. CONCLUSIONS

This study has allowed to build a 3-dimensional computer model of a fuel cell whose originality is to be able to compute the induced magnetic field inside and around the fuel cell. This model has been used in different steady state scenarios.

Among other things, it permits to compare the magnetic field maps of a good operating cell and a defect one. The final purpose is obviously to determine which defect can be easily

detected by magnetic measurement means and understand the precautions to be taken to achieve relevant measurements and diagnosis.

At a few tens of percent of rated current (a few amps to a few tens of amps for the studied cell), a defect at the cathode can be detected by measuring the tangential component of B with a sensor located closed to the cell. By contrast, a defect placed at the anode side produces a weak effect on the magnetic field B; it would be difficult to achieve a relevant diagnosis of such situation.

Experimental facility has to be led to demonstrate the scientific and technical feasibility of detecting a cell defect among a fuel cell stack. Specifically, the present study shows that, regarding the rated cell current density (approximately 0.5 to 0.7 A.cm⁻²), the resulted magnetic field does not exceed the 10⁻⁶ T range which can be challenging to measure especially considering that FC system auxiliaries may distort the measuring results. It is therefore essential to choose a Hall probe featuring a high sensitivity (in the order of mG) with relatively small active area due to the thickness of a single fuel cell.

According to all these considerations, the experimental setup has to be carried out so that the two current collectors do not disturb the measurement of the magnetic field induced by the fuel cell. One way to do so is to shield magnetically the fuel cell. Another promising way consists in correcting the measurements using the computation of auxiliaries' noises.

In sum, the simulation results allow to check the feasibility of diagnosis by means of magnetic field measurement and size the test bench and the associated sensors. This experimental stage is a key step and is the next phase of this work.

V. ACKNOWLEDGEMENT

We wish to acknowledge the research group SEEDS for partially fund this work.

REFERENCES

- [1] M. Hu, A. Gu, M. Wang, X. Zhu, L. Yu, Three dimensional, two phase flow mathematical model for PEM fuel cell: Part I. Model development, Energy Conversion and Management 45 (2004), 1861-1882.
- [2] M. Hu, A. Gu, M. Wang, X. Zhu, L. Yu, Three dimensional, two phase flow mathematical model for PEM fuel cell: Part II. Analysis and discussion of the internal transport mechanisms, Energy Conversion and Management 45 (2004), 1883-1916.
- [3] Y.-J. Sohn, M. Kim, T.-H. Yang, K. Kim, Numerical analysis of convective and diffusive fuel transports in high-temperature proton-exchange membrane fuel cells,
- [4] M. F. Serincan, and S. Yesilyurt. Transient Analysis of PEMFC at Start - Up and Failure, Fuel cell 2, (2006), 118-127
- [5] M. H. Daneshpajooh, E. A. Mason, E. H. Bresler and R. P. Wendt, Equation for membrane transport, Biophysical journal 15 (1975), 591-613.
- [6] C. W. Monroe and J. Newman, Onsager reciprocal relations for Maxwell-Stefan diffusion, American chemical Society 45 (2006), 5361-5367.
- [7] A. Parthasarathi, S. Srivivivasen, J.A. Appleby, C.R. Martin, Temperature dependence of electrode Kinetics of oxygen reduction at Platinum/Nafion interface-A microelectronic investigation, J. Electrochem. Soc. 139(9) (1992) 2530-2537.
- [8] T.E. Springer, T. A. Zawodzinski, S. Gottesfeld, Polymer electrolyte fuel cell model, J. Electrochem. Soc. 138 (8) (1991) 2334-2342